Journal of Electronic Materials
https://doi.org/10.1007/s11664-021-09158-2

TOPICAL COLLECTION: ELECTRONIC PACKAGING AND INTERCONNECTIONS 2021

Analysis of Pressure-Induced Whisker Nucleation and Growth in Thin Sn Films

Nupur Jain[1] · Xincheng Wang[1] · Piyush Jagtap[1] · Allan Bower[1] · Eric Chason[1]

Received: 22 April 2021 / Accepted: 9 August 2021

Abstract
A recent publication (Jagtap et al. Scr Mat 182:43, 2020) reported real-time observations of stress-driven whisker nucleation and growth in a thin film of Sn subjected to pressure on part of its surface. This paper describes a model of the experiment. Predicted whisker volume in the film adjacent to the loaded area is in good agreement with experimental measurements. The model also predicts correctly the variation of whisker density with distance from the punch at the end of the experiment but underestimates the rate of whisker nucleation during the first 50 h after the film is loaded. Comparison of model predictions with experiments provides clear evidence for a threshold stress for whisker growth, with an initial value of 17 MPa, which increases with whisker length to a saturated value of 22 MPa after whiskers reach a length of 19 μm. Implications for whisker growth in Sn films on Cu substrates are discussed.

Keywords Tin whisker · pressure induced whisker · stress relaxation · grain boundary diffusion

Introduction

Copper conductors used in printed circuit boards are usually coated with a thin film of tin or tin alloy, to improve solderability and reduce corrosion.[1] For reasons that are not fully understood, filamentary 'whiskers' are often observed to grow spontaneously from the surface of the film. The whiskers have a diameter comparable to the grain size of the film, and their length can exceed several millimeters. Long whiskers can cause short circuits between electronic components, so it is desirable to find ways to delay or prevent their formation. One approach is to alloy the tin with a small quantity of lead,[2] but environmental concerns make this undesirable.[3] Consequently, there is great interest in finding the causes of whiskers in Sn films.

There is strong experimental evidence suggesting that stresses in the film play an important role in whisker nucleation and growth.[4–7] Compressive stresses are induced in a Sn film on a Cu substrate when Cu diffuses into the Sn and reacts with it to form intermetallic particles.[4–6,8–10] Stresses caused by a thermal expansion mismatch between the film and substrate,[11–15] oxidation reactions[16] or mechanical loading,[4,17–22] can also drive whisker nucleation and growth. The precise mechanism for stress driven whisker growth has been the subject of some debate, but there is consensus that either short- or long-range gradients in stress drive atoms to diffuse into the base of whiskers, which are then extruded from the film.[1,6,8,21,23–25] Grain boundaries are one possible diffusion path. Sn films have a near-columnar grain structure, as illustrated schematically in Fig. 1a. Whiskers are often found above non-columnar grains.[1,14,26,27] Because the film is (on average) in a state of biaxial compression, the inclined (or horizontal) grain boundaries beneath the base of a whisker are subjected to a lower normal stress than the columnar grain boundaries. The chemical potential for grain boundary diffusion is proportional to the normal stress acting on the grain boundary,[28] so this difference in normal stress drives atoms to diffuse to the base of the whisker. Not all whiskers are found at non-columnar grains, however, and many other mechanisms for whisker nucleation and growth have been proposed.[1,3,5,23]

Experiments in which films are subjected to stresses under controlled conditions have helped to clarify and quantify the role of stress in driving whisker formation. Three approaches have been used to do this. Many previous studies have relied on the Sn-Cu reaction to drive whisker formation to generate the stress, which was measured by detecting the curvature of

✉ Nupur Jain
nupur_jain2@brown.edu

[1] School of Engineering, Brown University, Providence, RI 02912, USA

Published online: 05 September 2021

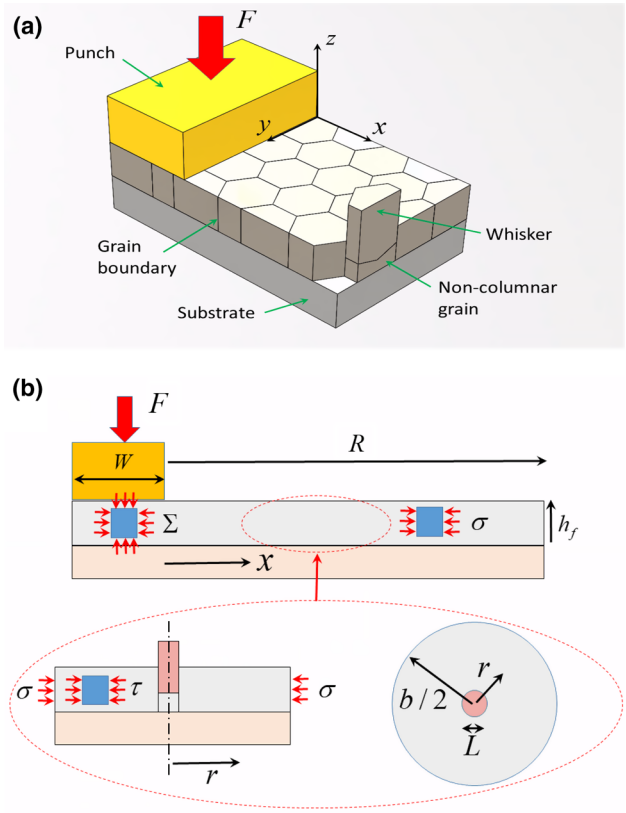

Fig. 1 Idealized model of stress-driven whisker growth: (a) Schematic showing a film with near-columnar grain structure loaded by a punch on its surface. A whisker forms by grain boundary diffusion into a non-columnar grain; (b) Theoretical model. At the scale of the punch, the film is idealized as a continuum subjected to average stress σ, which drives material to diffuse from under the punch into the surrounding film. At the microscale, the film is idealized as a periodic array of whiskers, subjected to an axisymmetric distribution of biaxial stress τ, which drives diffusion to the whisker, as well as dislocation creep. The area average of the micro-scale stress τ is equal to σ.

the substrate (see Ref. 23 for a review). A second approach, which allows the stress to be controlled more directly, is to heat the film.[11–15] This can subject a film to stress for a short period, typically on the order of 100 min, but dislocation creep and whisker growth relax the stresses, so it is not possible to subject a film to a constant stress for extended times using thermal loading. A third approach is to subject the film to a mechanical force.[4,17–21] A recent example can be found in Ref. 29 which used a clamping fixture to apply a constant pressure on an area of the film (Fig. 1). The fixture was small enough to fit inside a scanning electron microscope (SEM) chamber, so that the stress-driven whisker nucleation and growth next to the punch could be observed in real-time while the applied pressure was maintained on the Sn film. The experiment shows clearly that stress alone can cause whiskers to nucleate and grow, and provides quantitative data for the whisker density and whisker growth rate as functions of time. Some unexpected observations were also reported: firstly, whiskers were only observed in a region within 30 μm of the punch; and secondly, the whisker growth rate (quantified by the volume of material within whiskers per unit area of film surface) was found to decrease with time. One goal of the work reported in this paper is to explain these observations.

A drawback of using an indenter to introduce stress in the film is that, while the average pressure under the indenter can easily be determined and controlled, the state of stress in the area next to the indenter (where whiskers are observed) is unknown. Stresses build up in this area during the experiment, as material diffuses out from under the punch into the surrounding film, through grain boundaries. At the same time, the stresses relax by dislocation creep and whisker growth. A second goal of this paper is to calculate the stress distribution resulting from these processes. A third goal is to predict the rate of whisker nucleation and growth, and to compare the predictions with experimental measurement.

To this end, the next section describes a simple two-scale model of stress induced whisker nucleation and growth in a thin film that is loaded on its surface by a flat punch. The "Results and Discussion" section then presents the predictions of the model and conclusions are reported in the "Conclusions" section. A detailed description of the numerical procedures used to solve the governing equations listed in "Model Description" section can be found in the Appendix.

Model Description

Figure 1 shows a simple idealization of the experiment described in Ref. 29. Figure 1a shows a detailed schematic diagram of the microstructural features that play a role in whisker growth. Figure 1b shows the simplified idealization used in our calculations, which do not consider the grain structure in detail. The system consists of a film with thickness h_f of polycrystalline Sn on a rigid substrate. The film is in contact with a flat punch with width W and large (in the model, infinite) length out of the plane of the figure. In the experiment, a thin layer of glue (which has a low elastic modulus) was present between the surface of the punch and the film. We assume that this compliant layer ensures that a uniform pressure Σ acts on the surface of the film, and that creep deformation and diffusion in the film under the punch relaxes the stress to a state of uniform hydrostatic compressive stress, $\sigma_{xx} = \sigma_{yy} = \sigma_{zz} = -\Sigma$. The material adjacent to the punch is initially stress free, so that the pressure gradient causes material to flow through grain boundaries from underneath the punch into the adjacent film. As a result, a state of biaxial compressive stress $\sigma_{xx} = \sigma_{yy} = -\sigma(x,t)$ builds up in the film. Note that we take

compressive stress to be positive, to simplify plots and calculations. One goal of our calculation is to determine σ as function of position and time.

At the micro-scale, the film consists of an assembly of grains, with grain size L. Most grains are columnar, with near vertical grain boundaries. In between these, there are a few non-columnar grains with inclined or horizontal grain boundaries (Fig. 1a). These inclined grain boundaries are subjected to a lower normal stress than the vertical boundaries. This difference in normal stress drives material to diffuse into the inclined boundary. As material accumulates in this boundary, the grain above it is extruded from the film into a whisker. Note that grain boundary sliding must occur on vertical or inclined grain boundaries adjacent to or beneath the whisker. The sliding is resisted by a shear stress, which may prevent whisker growth altogether. We assume that whiskers will grow only if the stress in the film at the location of the whisker exceeds a critical magnitude τ_{crit}, which may increase as the grain boundaries slide, analogously to strain hardening. This critical stress is determined by the geometry and sliding resistance of the grain boundaries at the base of the whisker. Indirect evidence for a threshold stress has been observed in previous studies.[12,14] Calculations to be described in the next section show that the whisker growth rate in the film next to the punch is extremely sensitive to the value of the threshold stress, so that by fitting model predictions to the experiment, it is possible to determine precise values for the critical stress.

To quantify the whisker density, we define the area fraction of whiskers (the ratio of the surface area of whisker forming grains divided by the area of the film)

$$N \approx L^2 n \tag{1}$$

where n is the number of whiskers per unit area (a geometrical factor of order unity, which depends on the grain structure, has been omitted for simplicity). The spacing between whiskers $b \approx L/\sqrt{N}$ is assumed to be small enough that if we calculate the average stress in two regions surrounding neighboring whiskers, the difference in the average stress in the two regions will be small. New whiskers are assumed to nucleate when new non-columnar grain boundaries form in the film. This may occur, for example, when two adjacent columnar grain boundaries coalesce during grain growth.

The compressive stress within the grains causes them to deform, with a small elastic strain, together with a larger permanent plastic strain resulting from dislocation creep. This causes the grains to contract laterally, and increases their height, thereby relaxing the stress.

With this picture in mind, we view long-range diffusion of material through the grain boundary network (which takes place over distances of order 100 μm), and stress relaxation by creep and whisker growth (which is driven by stress gradients around individual whiskers, over distances between 5 and 15 μm), as occurring at two separate length-scales. It is convenient to model these two scales separately.

At a length-scale that is large compared to the whisker spacing, we consider only the *average* stress in the film, where the average is taken over an area that is larger than the spacing between whiskers. The average stress in the film obeys the plane version of Eq. 13 from Ref. 13

$$\frac{1}{3}\left(\frac{\Omega \overline{D}}{kT}\right)\frac{\partial^2 \sigma}{\partial x^2} = \frac{1}{M}\frac{\partial \sigma}{\partial t} + \dot{\varepsilon}^I(\sigma) \tag{2}$$

where M is the biaxial elastic modulus ($M = E/(1-\nu)$) (in terms of Young's modulus E and Poisson's ratio ν), Ω is the atomic volume of Sn, and $\overline{D}$ is an effective diffusion coefficient, defined as

$$\overline{D} = \frac{\delta_{\text{GB}} D_{\text{GB}} \exp(-Q_{\text{GB}}/kT)}{L} \tag{3}$$

where δ_{GB} is the thickness of the grain boundary diffusion layer; D_{GB} is the pre-exponential for the grain boundary diffusivity; Q_{GB} is the activation energy for grain boundary diffusion and L is the grain size. A detailed derivation and discussion of Eq. 2 can be found in Ref. 13: briefly, the term on the left-hand-side represents an in-plane strain (analogous to a thermal expansion) generated by the divergence of mass flux flowing from beneath the punch; the first term on the right-hand-side is an in-plane elastic strain rate, while $\dot{\varepsilon}^I(\sigma)$ in Eq. 2 represents the average in-plane uniaxial strain rate caused by the inelastic processes of dislocation creep and whisker growth. By the convention adopted here, a positive value of $\dot{\varepsilon}^I(\sigma)$ relaxes the compressive stress ($\partial\sigma/\partial t < 0$); therefore, it quantifies a contraction in the plane of the film, which is balanced by a corresponding increase in film thickness or whisker height. The necessary increase in film thickness or whisker height is calculated by analyzing the behavior of the film at the micro-scale, as described below.

The boundary conditions for the macro-scale average stress are

$$\sigma(x=0) = \Sigma; \quad \left.\frac{\partial \sigma}{\partial x}\right|_{x=R} = 0 \tag{4}$$

where Σ is the magnitude of the compressive stress state at the edge of the punch, and R is the distance between the edge of the punch and the edge of the specimen.

To solve Eq. 2, it is necessary to calculate the strain rate $\dot{\varepsilon}^I(\sigma)$, which quantifies the average strain rate caused by dislocation creep and whisker growth. For this purpose, we consider the behavior of the film at the micro-scale. We idealize the microstructure at a given distance from the edge of the punch as a periodic array of whiskers with spacing

$b = L/\sqrt{N}$, where L is the grain size, and $N(x)$ is the area fraction of whiskers. The whiskers relax the stresses in a small region surrounding them. We approximate the local biaxial stress surrounding a whisker by an axisymmetric distribution $\sigma_{xx} = \sigma_{yy} = -\tau(r)$, which is related to the average stress σ through

$$\sigma = \frac{8}{b^2 - L^2} \int_{L/2}^{b/2} \tau(r) r \mathrm{d}r \tag{5}$$

For a given value of the macro-scale stress σ, our goal is to calculate the local stress state τ near a whisker, the flux to the whisker, and the creep strain rate surrounding the whisker. This then allows the inelastic strain rate $\dot{\varepsilon}^I(\sigma)$ to be determined. The stress state τ around a whisker can be estimated by adapting the model of thermal stress-induced whisker growth described in Ref. 13. If the average stress σ is less than the critical stress τ_{crit} necessary to cause whiskers to grow, the stress surrounding the whisker is uniform. In this case, there is no diffusion of material to the whisker, and divergence in long-range flux of material from under the punch is accommodated by elastic deformation and dislocation creep within the grains. We use a standard power-law creep relation to model dislocation creep, in which the average inelastic strain rate is related to the micro-scale stress by

$$\dot{\varepsilon}^I(\sigma) = \frac{1}{2}\dot{\varepsilon}_0^p \exp(-Q_C/kT)\left(\frac{|\tau|}{\sigma_0}\right)^m \frac{\tau}{|\tau|} \tag{6}$$

The constants $\dot{\varepsilon}_0^p, \sigma_0, m, Q_C$ are a characteristic strain rate, flow stress, stress exponent and the activation energy in the thermally activated dislocation creep law (properties of the material), k is the Boltzmann constant, and T is the absolute temperature. If the stress exceeds the critical stress for whisker growth, a stress gradient develops around the whisker, which drives material to diffuse into the inclined grain boundaries at the whisker root. The average inelastic strain rate is then related to the stress by

$$\dot{\varepsilon}^I(\sigma) = -\frac{1}{3}\left(\frac{\Omega\overline{D}}{kT}\right)\left(\frac{\partial^2\tau}{\partial r^2} + \frac{1}{r}\frac{\partial\tau}{\partial r}\right) + \frac{1}{2}\dot{\varepsilon}_0^p \exp(-Q_C/kT)\left(\frac{|\tau|}{\sigma_0}\right)^m \frac{\tau}{|\tau|} \tag{7}$$

The first term on the right-hand-side in Eq. 7 quantifies the strain rate caused by grain boundary diffusion towards the whisker, while the second term represents dislocation creep. Note that in both Eqs. 6 and 7, we have taken compressive stress to be positive.

The boundary conditions for the stress state in Eq. 7 are

$$\left.\begin{array}{ll} \frac{\partial\tau}{\partial r} = 0 & |\tau| < \tau_{\mathrm{crit}} \\ \tau\frac{\partial\tau}{\partial r} > 0 & |\tau| = \tau_{\mathrm{crit}} \end{array}\right\} \quad r = \frac{L}{2} \quad \frac{\partial\tau}{\partial r} = 0 \quad r = b/2 \tag{8}$$

The first of these conditions ensures that the stress at the whisker is less than or equal to the critical stress for whisker growth, and that whiskers grow under a compressive stress and shrink under a tensile stress. The second condition enforces zero flux at the boundary between neighboring whiskers, which is required by symmetry. Given the average stress σ, Eqs. 5 and either 6 or 7 may be solved for τ and $\dot{\varepsilon}^I(\sigma)$, providing the connection between the macroscopic and microscopic length-scales. The numerical procedure used to do this is described in more detail in the Appendix.

The whisker growth rate is related to the stress by

$$\frac{\mathrm{d}h_w}{\mathrm{d}t} = \left(\frac{4h_f\Omega\overline{D}}{LkT}\right)\left.\frac{\partial\tau}{\partial r}\right|_{r=L/2} \tag{9}$$

where h_{f} is the film thickness, while the rate of change of whisker volume per unit area of the film is

$$\frac{\mathrm{d}V_w}{\mathrm{d}t} = N\frac{\mathrm{d}h_w}{\mathrm{d}t} = N\left(\frac{4h_f\Omega\overline{D}}{LkT}\right)\left.\frac{\partial\tau}{\partial r}\right|_{r=L/2} \tag{10}$$

Experiments show that whiskers next to the punch initially grow rapidly, but their growth rate decreases with time and may eventually drop to zero. We attribute this to an increase in the slip resistance of the grain boundaries at the base of the whisker, which may occur as a result of an increase in the shear strength of the boundaries, or a change in the orientation or topology of the grain boundaries as a result of grain growth. We model these processes by assuming that the critical stress for whisker growth increases with the height of the whisker, using a simple linear hardening relation

$$\tau_{\mathrm{crit}} = \begin{cases} \tau_0 + h_w(\tau_1 - \tau_0)/h_0 & h_w \le h_0 \\ \tau_1 & h_w \ge h_0 \end{cases} \tag{11}$$

where τ_0, τ_1 are the initial and saturated critical stresses for whisker growth, and h_0 is a characteristic whisker height.

The mechanism responsible for nucleating whiskers is not fully understood. Chason et al.[30] have suggested that non-columnar grains may be formed by the coalescence of neighboring grain boundaries during grain growth. They show that experimental measurements of whisker nucleation rates during thermal cycling of Sn films can be fit by a thermally activated nucleation model of the form

$$\frac{\mathrm{d}N}{\mathrm{d}t} = \left(1 - \frac{N}{N_{\mathrm{sat}}}\right)\beta_c \exp\left(-\frac{\Delta G_{\mathrm{ref}} + U(\sigma)}{kT}\right) \tag{12}$$

Here, β_c is an attempt frequency; N_{sat} is the saturated area fraction of whiskers after all nucleation sites have

been exhausted; ΔG_{ref} is the activation energy for nucleation at the reference stress value σ_2, and

$$U(\sigma) = -U_0 \left[\frac{(\sigma - \sigma_1)}{(\sigma_2 - \sigma_1)} \right] \tag{13}$$

with U_0, σ_1, σ_2 three constants, is a linear fit to the measured stress dependence of the activation energy.

Values for relevant parameters and material properties in the model are listed in Table I. Many material properties can be determined from literature data, as indicated in the table. The material properties $\dot{\epsilon}_0^p, \sigma_0, m, Q_C$ that govern creep, and the parameters $\Delta G_{\text{ref}}, \beta_c, U_0, \sigma_1, \sigma_2$ that govern whisker nucleation, were determined by fitting predictions of the model to the experimental data reported in Ref. 11. In this experiment, a thin Sn film on a Si substrate was first heated at 2°C/min to a prescribed temperature (45°C, 55°C or 78°C). The film was then held at constant temperature for a further 2 h. The stress in the film was determined by measuring the curvature of the substrate. The whisker density was measured at the same time. The properties governing creep were determined by fitting the predicted peak stress to the experimental data. The parameters governing whisker nucleation were determined by fitting the predicted peak whisker nucleation (which occurs at the maximum temperature) to experimental data. A comparison of the model predictions with the data from the thermal cycling experiments is shown in Fig. 2. Figure 2a plots the stress as a function of time, while Fig. 2b plots the whisker nucleation rate. Note that the time scale on the measured whisker nucleation rate was adjusted to correct for the fact that nucleation sites can only be detected after whiskers reach a length of 0.4 μm. In the figure, the measured times were adjusted so that the peak nucleation rate occurs at the same time in predictions and measurements. It was found that the value of the attempt frequency β_c determined from the thermal cycling experiments substantially underestimated the measured whisker density in the punch experiment. Consequently, β_c was determined by fitting to the measured whisker density in the punch experiment, as discussed in more detail in the next section.

The grain boundary diffusivity and threshold stress for whisker growth cannot be determined precisely from thermal relaxation experiments. Consequently, the activation energy for grain boundary diffusion was taken from data taken during an electromigration experiment reported in Ref. 31 while the pre-exponential was fit to data from the punch experiment. The fit yields a value within a factor of 4 of the value reported in Ref. 31. Similarly, the initial and saturated threshold stresses for whisker growth, and the characteristic length in the hardening rate for threshold stress, were fit to data from the punch experiment.

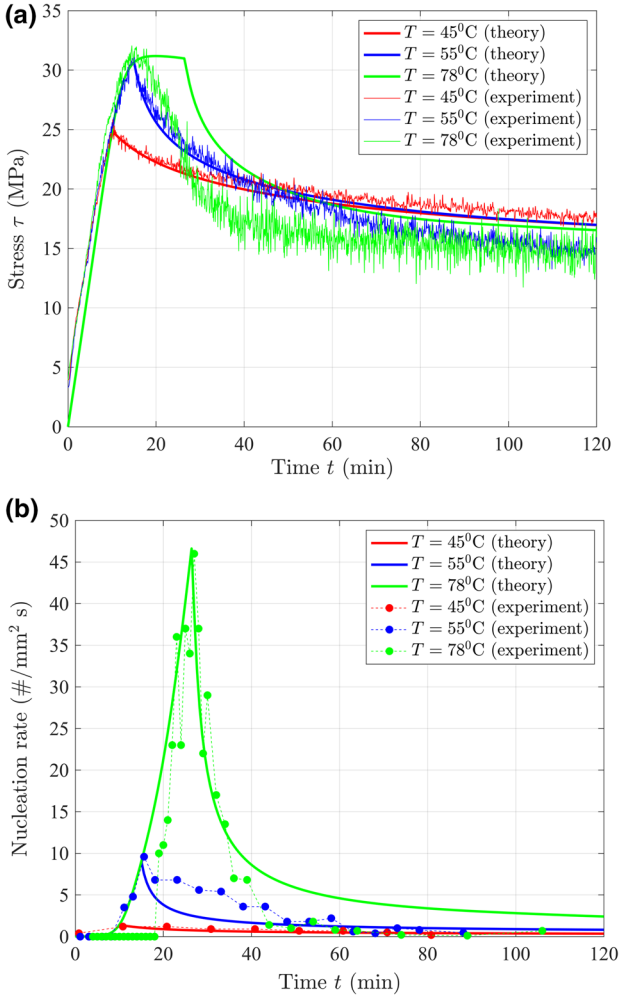

Fig. 2 Comparison of model predictions with experimental measurements from Ref. 11 of (a) stress relaxation and (b) whisker nucleation rate in a thin Sn film that was heated from room temperature at 2°C/min to a prescribed temperature, and then held at constant temperature. The data are used to calibrate the model.

Results and Discussion

The model described in the preceding section predicts the variation of mean stress σ, the whisker area fraction N (or equivalently, the number of whiskers per unit area N/L^2), the whisker height h_w and volume V_w as functions of position and time. Predictions of whisker density and volume may be compared with experimental measurements.

It is helpful to begin by examining the stress distribution in the film, which is plotted in Fig. 3. Figure 3a shows the stress near the edge of the punch (whiskers are observed experimentally in the region $0 < x < 30$ μm), while Fig. 3b shows the stress over the full width of the specimen. Recall

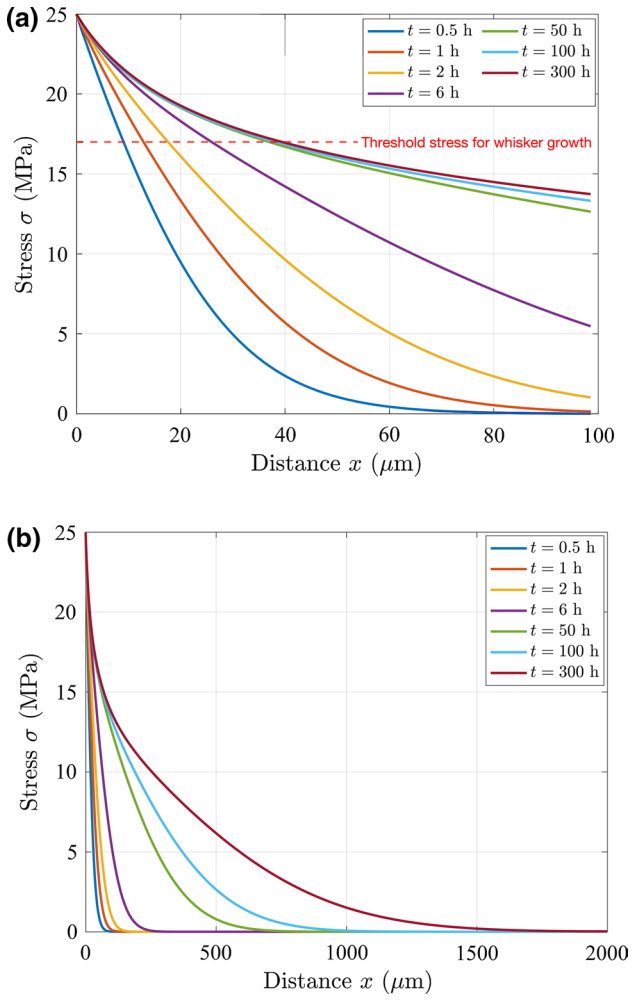

Fig. 3 Predicted variation of area-averaged (compressive) stress σ with distance x from the edge of the punch and time. (a) Stress state near the punch edge, where whiskers are observed; (b) Stress state over the full width of the specimen. Note that the stress field in the region where whiskers form reaches steady state in approximately 50 h.

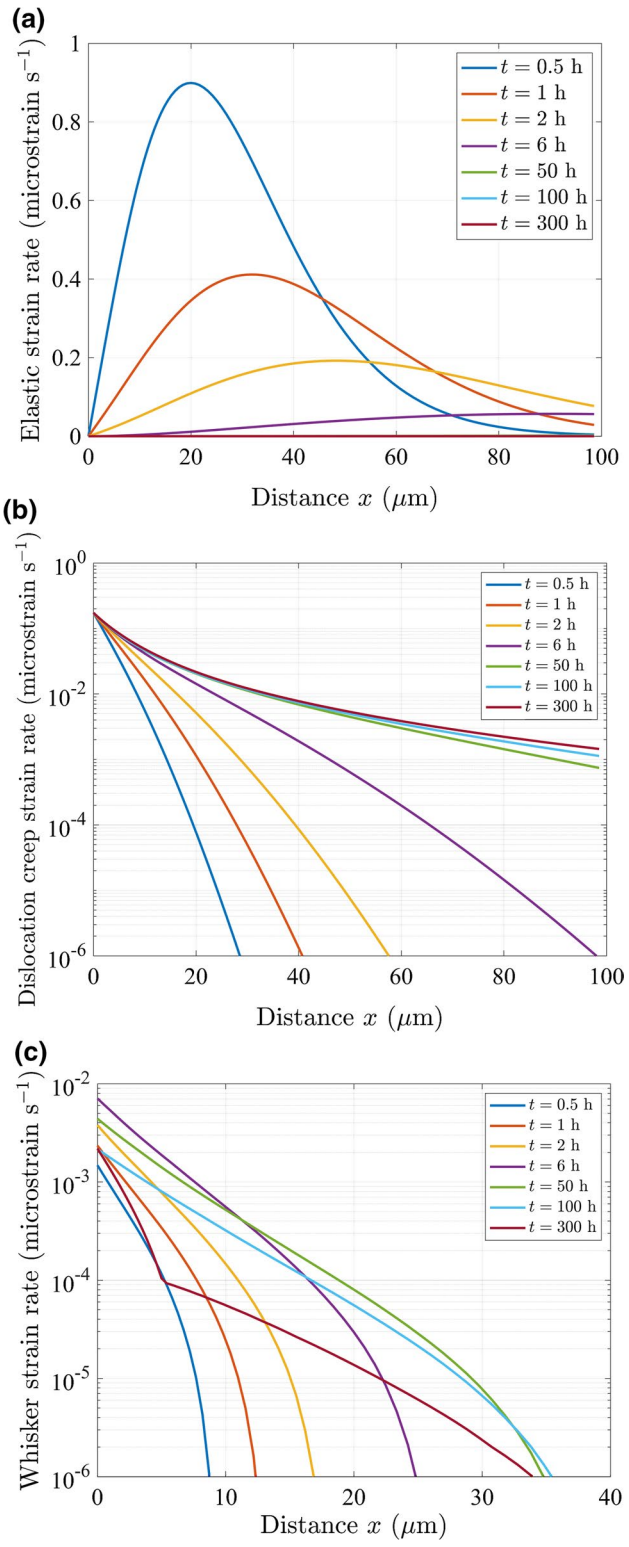

Fig. 4 Predicted contributions to the total strain rate in the film from (a) elastic deformation, (b) dislocation creep and (c) whisker growth. Dislocation creep is the dominant mechanism for relaxing stress once the stress reaches steady-state.

that a positive value of σ denotes a compressive stress. At time $t = 0$, the film outside the punch is stress free, while the film below the punch is subjected to the imposed 25 MPa pressure. The stress gradient drives material to diffuse from under the punch into the surrounding film, and as a result, compressive stresses develop adjacent to the punch. Predictions suggest that the stresses in the region $0 < x < 80$ μm reach steady-state in approximately 50 h. Further from the punch, the stresses continue to build up until the end of the experiment, at 300 h.

The stresses reach steady-state when the rate of stress generation by grain boundary diffusion is equal to the rate of stress relaxation by dislocation creep and whisker growth. To determine which of the two stress relaxation mechanisms dominates, Fig. 4 plots (a) the variation of

elastic strain rate $\dot{\varepsilon}^e = (\mathrm{d}\sigma/\mathrm{d}t)/M$, (b) the dislocation creep strain rate $\dot{\varepsilon}^p$, and (c) the contribution to the total strain rate $\dot{\varepsilon}^I$ from the growth of whiskers, as functions of distance from the punch edge and time. Whisker growth clearly provides a negligible contribution to stress relaxation throughout the experiment. At early times ($t < 6$ h), as the stress in the film builds up, elastic deformation is the dominant deformation mechanism throughout the film. In the region near the punch ($x < 100$ μm), dislocation creep is the dominant mechanism for relaxing stress once the stress reaches steady state ($t > 50$ h). Further away from the punch ($x > 100$ μm), both elastic deformation and dislocation creep continue to contribute approximately equal contributions to the total strain rate throughout the duration of the experiment ($t < 300$ h).

Our model assumes that whisker nucleation is a thermally activated process, driven by stress. The variation of whisker density resulting from this process with distance from the punch and time is displayed in Fig. 5. Experimental data from Ref. 29 are also shown for comparison. Note that the material properties in the nucleation model were fit to the experimentally measured whisker density at 300 h. The model can clearly predict the spatial distribution of whisker density at this time correctly, but does not give a good fit to the evolution of whisker density with time. In the experiments, whiskers are observed to nucleate rapidly during the first 5–10 h, and thereafter the nucleation rate is slow. The model predicts that the nucleation rate increases with time, as the stress builds up around the punch to the steady state distribution. No model in which whisker nucleation rate is a monotonically increasing function of stress can fit the experimental data. A phenomenological relation of the form $\mathrm{d}N/\mathrm{d}t = \beta_1 + \beta_2(\mathrm{d}\sigma/\mathrm{d}t)$, where β_1, β_2 are two constants (which could depend on stress) would fit the observations, but it is not clear what physical process would lead to nucleation kinetics of this form.

Once whiskers have nucleated, they continue to grow if the stress exceeds the threshold stress for whisker growth. Figure 6a shows the predicted variation of whisker length with distance from the punch and time. Whiskers only grow in the region within 30 μm of the punch, where the stress exceeds the initial threshold stress for whisker growth. The whisker growth rate is fastest near the punch, and progressively decreases with distance. In addition, because the threshold stress for whisker growth increases with whisker height, the whisker growth rate decreases with time. This can be seen more clearly in Figure 6b, which shows the whisker growth rate as a function of position. Whisker growth drops below 0.05 μm/h beyond 5 μm from the edge of the punch,

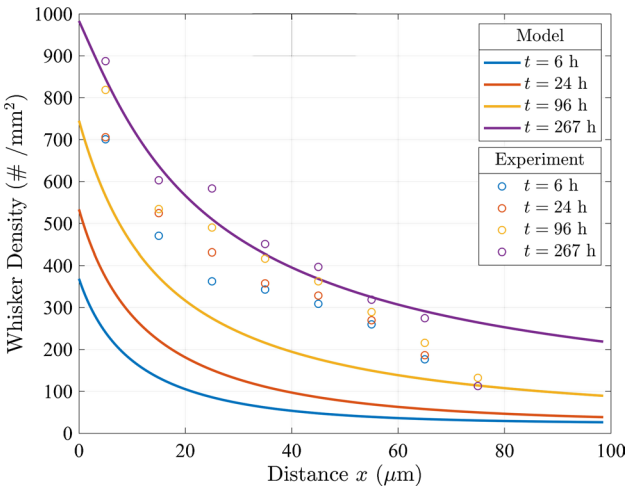

Fig. 5 Comparison of measured[29] and predicted whisker density as a function of distance from the edge of the punch and time. The model predicts the spatial variation of whisker density at 267 h correctly, but underestimates the rate of whisker nucleation for $t < 100$ h.

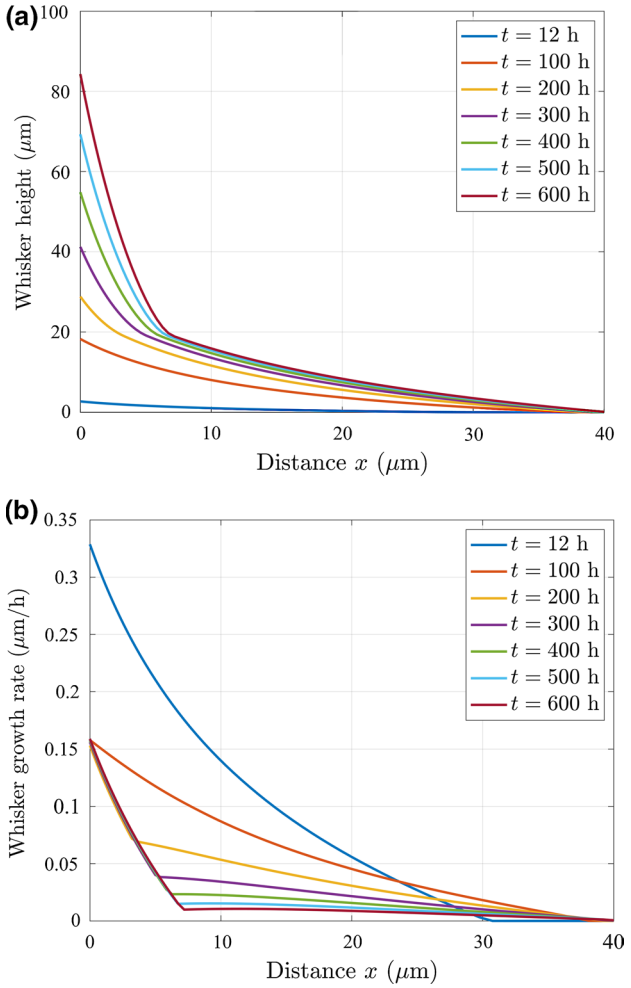

Fig. 6 Predicted variation of (a) whisker height and (b) whisker growth rate with distance from the edge of the punch, as a function of time. Whiskers grow only in the region $0 < x < 35$ μm, where stresses exceed the threshold stress for whisker growth. The rate of whisker growth gradually decreases with time, because the threshold stress increases with whisker length.

where the stress is below the saturated value of threshold stress. In this region, the whisker growth eventually ceases. Nearer the punch, the stress exceeds the saturated value of threshold stress, and whiskers grow at a constant rate.

The predicted whisker growth rate may be compared directly with experiment. Experiments cannot directly measure the whisker density at a point on the surface, since a finite number of whiskers must be counted to determine the volume. Ref. 29 measured the average whisker volume over finite 10 μm wide strips of the surface as functions of time. The average whisker volume in these regions can be predicted by averaging the data displayed in Fig. 6. The predictions are compared to experiment in Fig. 7. The rate of change of threshold stress with whisker height in the model was fit to the measured whisker height with time in the region $x < 10$ μm, so in this region the agreement is expected. The model also predicts correctly the whisker volume in the region 10 μm $< x <$ 20 μm. It underestimates the whisker growth rate for 20 μm $< x <$ 30 μm, but the predictions for this region remain within the scatter in experimental data.

It is also interesting to predict the influence of test conditions and material properties on the stress distribution and whisker growth rate. For this purpose, it is helpful to note that the relationships between stress, whisker volume per unit area of film, and whisker height can be expressed in dimensionless form as

$$\left\{\frac{\sigma}{\Sigma}, \frac{MV_w}{\Sigma h_f}, \frac{Mh_w}{\Sigma h_f}\right\} = F\left\{\frac{t}{t_0}, \frac{x}{L}, \Gamma, m, \frac{\tau_0}{\Sigma}, \frac{\tau_1}{\Sigma}, \frac{h_0}{L}, N_0, N_{sat}, \frac{U_0}{kT}, \frac{\sigma_1}{\Sigma}, \frac{\sigma_2}{\Sigma}, t_0\beta_c, \frac{\Delta G_{ref}}{kT}\right\} \tag{14}$$

where

$$t_0 = \frac{kTL^3}{M\Omega D_{GB}\delta_{GB}\exp(-Q_{GB}/kT)} \tag{15}$$

is the characteristic time for stress relaxation by grain boundary diffusion, while

$$\Gamma = \frac{kTL^3\dot{\varepsilon}_0^p\exp(-Q_C/kT)}{\Omega\Sigma D_{GB}\delta_{GB}\exp(-Q_{GB}/kT)}\left(\frac{\Sigma}{\sigma_0}\right)^m \tag{16}$$

is a dimensionless constant that can be interpreted physically as the ratio of the characteristic rate of stress relaxation by dislocation creep, to the rate of stress relaxation by grain boundary diffusion. The 5th–7th parameters in Eq. 14 are dimensionless measures of the initial and saturated values of threshold stress for whisker growth and the rate of hardening of the threshold stress. The remaining parameters quantify the rate of whisker nucleation.

For parameter values listed in Table I, the time constant $t_0 = 19s$ at room temperature (25°C), and ranges from $0.5s < t_0 < 102s$ for temperatures between 100°C and 0°C. The results in Fig. 3 suggest that the stresses within 100 μm of the punch reach steady state after approximately 10 h at room temperature, which rises to 100 h at 0°C and drops to 5 min at 100°C. The times scale with the cube of the grain size and will be 30 times faster in a film with 1 μm grain size. These times are short compared to the time required for whiskers to form, suggesting that under most test conditions of practical interest, whisker growth is driven by the steady-state stress field. We, therefore, focus on the influence of test conditions and material properties on the steady-state stress field and the resulting whisker growth rates.

The parameter Γ defined in Eq. 16 has the most significant influence on the stress state. For representative values of loads, temperatures and material properties, Γ ranges between $0 < \Gamma < 0.01$. It increases with grain size and punch stress, and decreases with temperature. The steady-state stress distribution for several values of Γ in the range of interest is plotted in Fig. 8. The values of the remaining parameters in Eq. 14 may be calculated using the data listed in Table I. The results are shown at a normalized time $t/t_0 = 5.8 \times 10^4$, which corresponds to 300 h at room temperature for a film with properties listed in Table I (there is no significant change in the stress distribution for $t/t_0 > 5.8 \times 10^4$). The most important conclusion to be drawn from Fig. 8 is that stresses tend to decay more rapidly with distance from the punch for large values of Γ. This is because dislocation creep becomes a more effective stress relaxation mechanism for large Γ. Equation 16 shows that Γ increases with the grain size of the

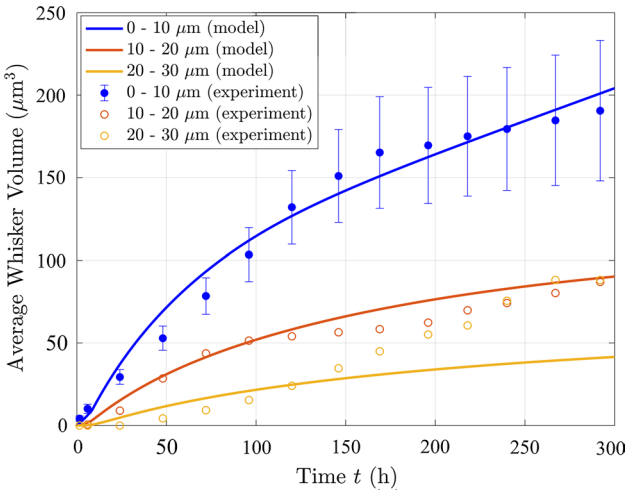

Fig. 7 Comparison of measured[29] and predicted whisker volume as a function of distance from the edge of the punch. Model predictions are within the scatter in the experimental data.

Table I Values for parameters and material properties used in simulations of whisker growth driven by mechanical pressure

Film thickness h_f	4 μm[1]
Punch pressure Σ	25 MPa
Punch width W	1.5 mm
Film width R	2 mm
Grain size L	3 μm[1]
Temperature T	298K
Boltzmann constant k	1.381×10^{-23} J K^{-1}
Atomic volume of Sn Ω	2.7×10^{-29} m^3
Young's modulus of Sn E	50 GPa
Poisson's ratio of Sn ν	0.36
Characteristic strain rate for dislocation creep $\dot{\epsilon}_0$	0.096 s^{-1}
Characteristic stress for dislocation creep σ_0	16.5 MPa
Stress exponent for dislocation creep m	8
Activation energy for dislocation creep Q_c	0.425 eV
Pre-exponential for grain boundary diffusion D_{GB}	1.6×10^{-3} m^2 s^{-1}
Activation energy for grain boundary diffusion Q_{GB}	0.5 eV
Grain boundary diffusion layer thickness δ	0.5 nm
Initial threshold stress for whisker growth τ_0	17 MPa
Saturated threshold stress for whisker growth τ_1	22 MPa
Characteristic length for hardening of threshold stress h_0	19 μm
Initial whisker density $n_0 = N_0/L^2$	20 mm^{-2}
Saturated whisker density $n_{sat} = N_{sat}/L^2$	1100 mm^{-2}
Activation energy for whisker nucleation at reference stress ΔG_{ref}	0.85 eV
Characteristic energy for stress driven whisker nucleation U_0	0.08 eV
Reference stress for whisker nucleation σ_1	18 MPa
Characteristic stress for whisker nucleation σ_2	35 MPa
Attempt frequency for whisker nucleation β_c	1.89×10^8 s^{-1}

[1]The film in thermal cycling experiments (Fig. 2) has a grain size of 2 μm and thickness of 2.5 μm

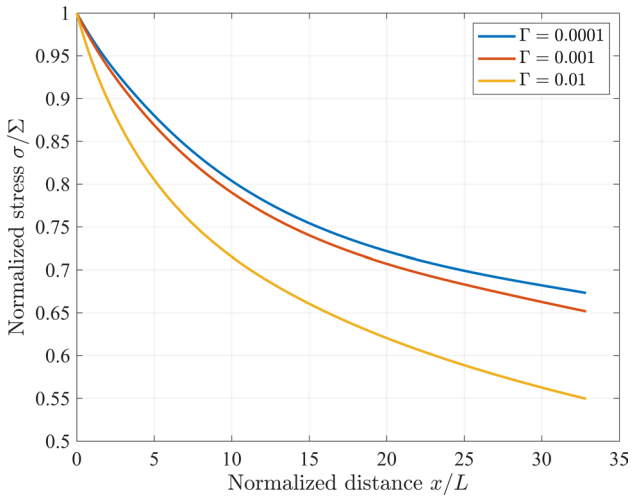

Fig. 8 The variation of normalized stress with normalized distance from the edge of the punch, for several values of the parameter Γ defined in Eq. 16. Results are shown for normalized time $t/t_0 = 5.8 \times 10^4$. The remaining parameter values are listed in Table I. Note that stresses decay more quickly with distance for large values of Γ.

film, with the force acting on the punch, and decreases with temperature. This suggests that whiskers will be observed further away from the punch for a film with small grain size, and at high temperatures. Increasing the force on the punch increases the stress near the edge of the punch, but at the same time the region of large stress tends to be confined to a progressively reducing area next to the punch. These observations are confirmed by Fig. 9, which shows the variations of (a) dimensionless whisker length and (b) dimensionless whisker growth rate with distance from the punch, for several values of Γ. Results are shown for $t/t_0 = 3 \times 10^5$. For this large value of dimensionless time, the threshold stress for whisker growth has hardened to its saturated value in a region adjacent to the punch. In this region, whiskers continue to grow at a constant rate. Further from the punch, the threshold stress has hardened sufficiently to reduce the whisker growth rate to zero. In this region Fig. 9a shows the final length of the whiskers.

The threshold stress for whisker growth has a very significant influence on the whisker growth rate (but has no perceptible influence on the stress distribution, since dislocation creep, rather than whisker growth, is the dominant stress

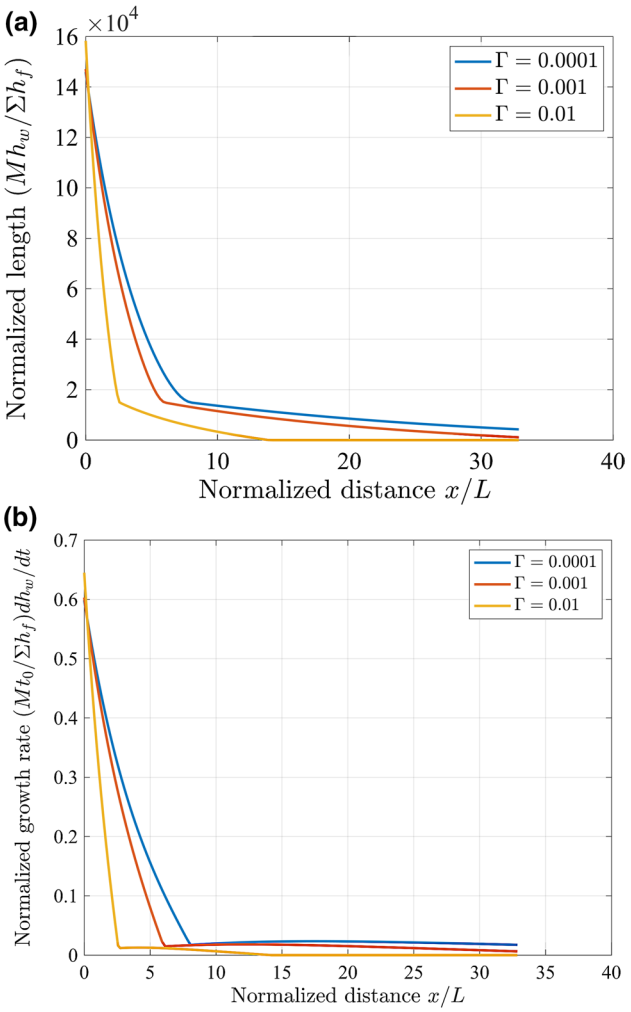

Fig. 9 The variation of normalized (a) whisker length and (b) whisker growth rate with normalized distance from the edge of the punch, for several values of the parameter Γ defined in Eq. 16. Results are shown for normalized time $t/t_0 = 5.8 \times 10^4$. The remaining parameter values are listed in Table I. With increasing Γ, the width of the region where whiskers grow decreases.

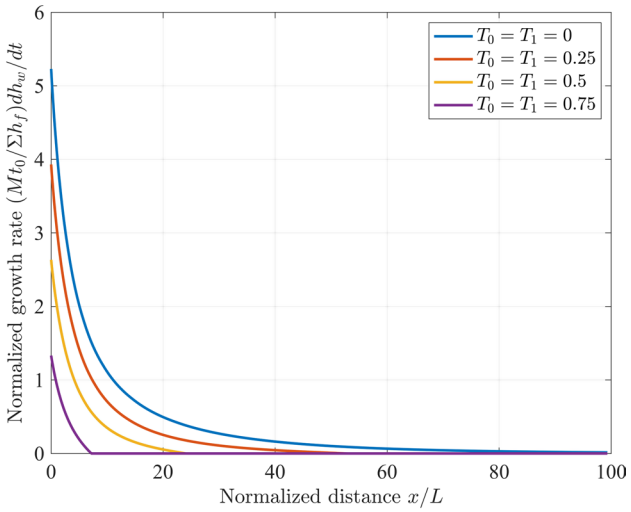

Fig. 10 The variation of normalized whisker growth rate with normalized distance from the edge of the punch, for several values of the normalized threshold stress for whisker growth T_0, T_1 defined in Eq. 16. Since $T_0 = T_1$, the threshold stress is independent of whisker length and whiskers grow at a constant rate once stresses reach steady state. Results are shown for normalized time $t/t_0 = 5.8 \times 10^4$. The width of the region where whisker growth is observed is very sensitive to the threshold stress.

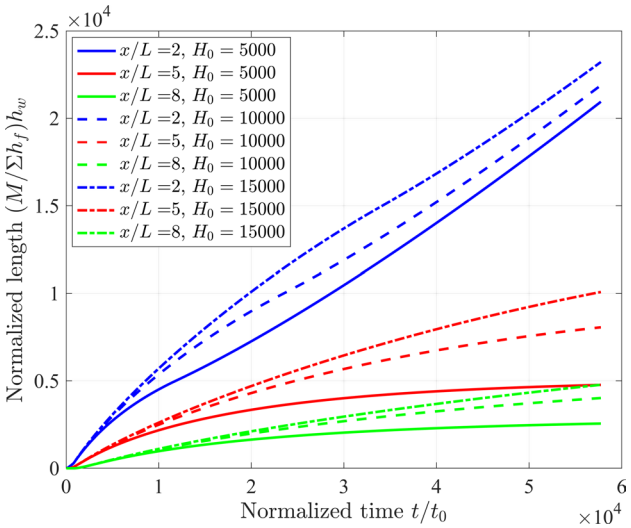

Fig. 11 The variation of normalized whisker length with normalized time, for three different distances from the edge of the punch. Results are shown for normalized threshold stress for whisker growth $T_0 = 0.71, T_1 = 0.8$ and three different values of hardening rate H_0. Higher rates of hardening reduce the growth rate.

relaxation mechanism). To illustrate this, Fig. 10 shows the predicted whisker growth rate in a film with a constant threshold stress (i.e. the threshold stress is independent of whisker length). With a constant threshold stress, whiskers continue to grow at a constant rate once the stress near the punch reaches steady state (Fig. 10 shows the steady-state whisker growth rate). The simulations predict that without a threshold stress for whisker growth whiskers will grow even at large distances from the punch. Since the stress decreases gradually with distance next to the punch, a small change in threshold stress produces a large change in the distance over which whiskers form. Measuring this distance consequently provides a sensitive probe of the threshold stress. The influence of hardening of the threshold stress is illustrated in Fig. 11, which shows the predicted whisker length as a function of time. Higher rates of hardening slow down whisker growth, and for large distances from the punch ($x/L > 5$) may stop whiskers from growing.

Evidence for a threshold stress for whisker growth was previously reported by Pei et al.[11]based on thermal stress

relaxation experiments. They estimated a value of 15 MPa for the threshold stress, which is very close to the value of 17 MPa obtained from the punch experiment. Here, we have also assumed that the threshold stress increases in proportion to the whisker length, before saturating at a value of 22 MPa. This increase in threshold stress is a possible explanation for the decrease in whisker growth rate with time observed in the experiments. There are other possible explanations for this decrease, however. For example, if matter flowing into the non-columnar grain boundaries is deposited equally on the whisker grain and the grain below it, the grain boundary would migrate up through the film at a speed equal to half the whisker growth rate. Eventually, the grain boundary reaches the surface of the film and whisker growth stops, unless a new non-columnar grain boundary nucleates at the whisker base. Grain boundaries are sometimes observed inside whiskers,[23] and may form by this process. Single-crystal whiskers with length greatly exceeding the film thickness are also common, however, suggesting that non-columnar grain boundaries are not always mobile. In addition, the experiments found large variations in whisker growth rate, as indicated by the error bars in Fig. 7. In the model, all whiskers that are the same distance from the punch are assumed to grow at the same rate. In the experiments, this is not the case: some whiskers stop growing altogether, while others continue to grow for as long as the experiment continues.[29] The reasons for these variations are not known. They may be caused by microstructural variations, which lead to variations in local material properties such as the threshold stress for whisker growth. They may also be caused by changes in the microstructure of the film resulting, e.g., from grain growth. The model used here does not capture these variations, and predicts only the average behavior of a population of whiskers. Extending the model to consider statistical variations in whisker growth rates and additional experiments to clarify their microstructural origins, will be fruitful areas for future study.

Next, we examine the influence of the whisker nucleation kinetics. We focus on the influence of the stress dependence of the activation energy U. Simulations show that the nucleation kinetics has a negligible influence on the stress distribution. This is to be expected, since dislocation creep is the main stress relaxation mechanism, with whisker growth providing a negligible additional contribution. Figure 12 shows the influence of the activation energy for whisker nucleation on (a) the whisker density and (b) the normalized whisker volume per unit area, at a dimensionless time $t/t_0 = 5.8 \times 10^4$. Larger values of U_0 make the nucleation rate more sensitive to stress, therefore, increasing the gradient of the whisker density

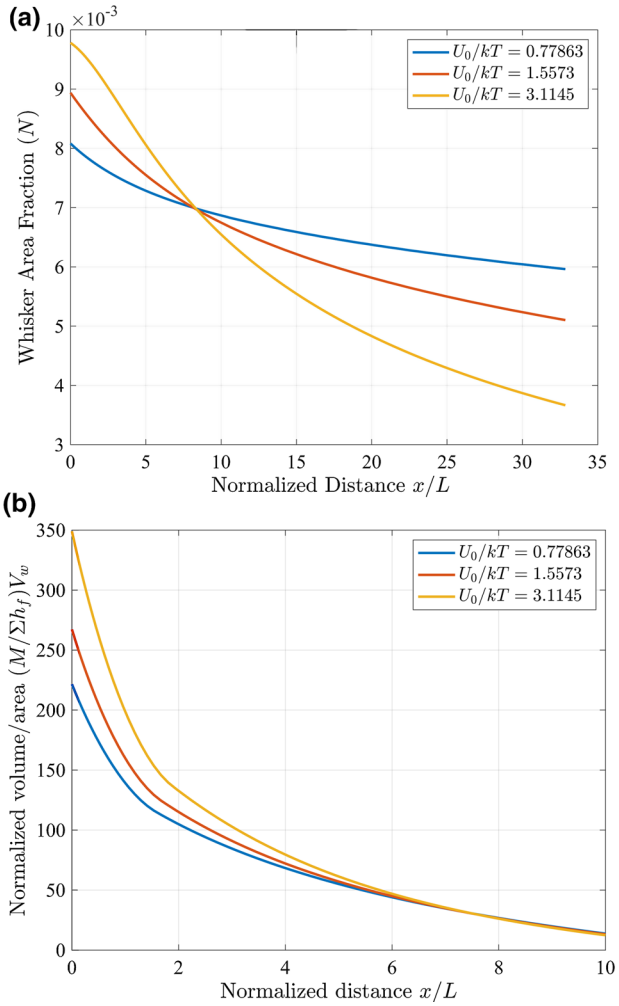

Fig. 12 The variation of (a) whisker area fraction and (b) normalized whisker volume per unit area with distance from the edge of the punch, at a dimensionless time $t/t_0 = 5.8 \times 10^4$. Results are shown for several values of the stress-dependent activation energy for nucleation U_0/kT. Larger values of U_0/kT increase the whisker density near the punch and decrease it further from the punch.

adjacent to the punch. The larger density of whiskers then leads to a larger whisker volume per unit area.

Finally, we consider the implications of the model predictions on whisker nucleation and growth in Sn films on Cu substrates used in electronic circuits. In this system, Cu preferentially diffuses into the Sn and reacts with it to form an intermetallic compound (IMC, primarily Cu_6Sn_5 at room temperature[32]). The formed intermetallic compound has a larger volume than the volume of Sn that it replaces, which introduces an average volumetric strain rate in the film

$$\frac{\mathrm{d}e}{\mathrm{d}t} = \left(1 - \frac{5\omega_{\mathrm{Sn}}}{11\omega_{\mathrm{IMC}}}\right)\frac{1}{h_{\mathrm{f}}}\frac{d(V_{\mathrm{IMC}}/A_f)}{\mathrm{d}t} \approx \frac{0.31}{h_{\mathrm{f}}}\frac{d(V_{\mathrm{IMC}}/A_{\mathrm{f}})}{\mathrm{d}t} \tag{17}$$

where $\omega_{Sn}, \omega_{IMC}$ are the molar volumes of Sn and intermetallic compound, respectively, and V_{IMC}/A_f is the volume of the intermetallic compound per unit area of film. The molar volumes are taken from Ref. 33, where $\omega_{Sn} = 16.3$ cm^3/mol and $\omega_{IMC} = 10.7$ cm^3/mol are calculated based on the composition of 5/11 atomic fraction Sn; therefore, 1 mol of IMC replaces an initial Sn volume of (5/11) $\omega_{Sn} = 7.4$ cm^3/mol. Experiments suggest that the rate of change of intermetallic volume lies in the range 0.5 nm/h $< (1/A_f)\mathrm{d}V_{IMC}/\mathrm{d}t <$ 100 nm/h.[23] The stress distribution around a representative whisker in the film, and the whisker growth rate, can be found by substituting $\dot{\varepsilon}^I(\sigma) = (1/3)(\mathrm{d}e/\mathrm{d}t) - (1/M)(\mathrm{d}\tau/\mathrm{d}t)$ in Eqs. 6–10.

Figure 13 shows the predicted (a) stress, (b) whisker density and (c) average whisker length for a film with properties listed in Table I, for three different values of IMC growth rate. In each case, the whisker density rapidly saturates. The predicted whisker density is unlikely to be accurate, however, in view of the discrepancies between theory and experiment. Moreover, the saturated whisker density cannot be determined accurately from the data in the punch experiment or thermal cycling tests. Fortunately, the predicted stress and whisker length are not strongly sensitive to the saturated whisker density. For the lowest IMC growth rate of 1 nm/h, the stress in the film builds up slowly and saturates at a value slightly higher than the initial threshold for whisker growth. The predicted whisker length is below 1 μm after 100 h, and the whisker will eventually stop growing. For intermediate IMC growth rate of 5 nm/h, the stress builds up more quickly and asymptotically to a value between the initial and saturated value of the threshold stress. Whisker growth is slow, and the whisker does not reach the 19-μm length required to reach the saturated value of threshold stress. Consequently, whiskers eventually stop growing for this case. Finally, for the highest IMC growth rate, the stress builds up quickly to a value that exceeds the saturated value of threshold stress. For this case, whisker growth will continue indefinitely. The predicted whisker heights are comparable to those observed in experiments.[23,34]

It is straightforward to calculate the conditions that lead to unlimited whisker growth. If no whisker growth occurs, the steady-state stress (for a constant rate of intermetallic growth) is given by

$$\tau_{creep} = \sigma_0 \left[\frac{\frac{2}{3}\left(1 - \frac{5\omega_{Sn}}{11\omega_{IMC}}\right)\frac{1}{h_f}\frac{\mathrm{d}(V_{IMC}/A_f)}{\mathrm{d}t}}{\dot{\varepsilon}_0^p \exp(-Q_C/kT)} \right]^{1/m} \tag{18}$$

If $\tau_{creep} < \tau_0$ (where τ_0 is the initial threshold stress for whisker growth) no whiskers will grow. If $\tau_{creep} < \tau_{sat}$, where τ_{sat} is the saturated threshold stress for whisker growth, whiskers will grow initially, but will stop growing before

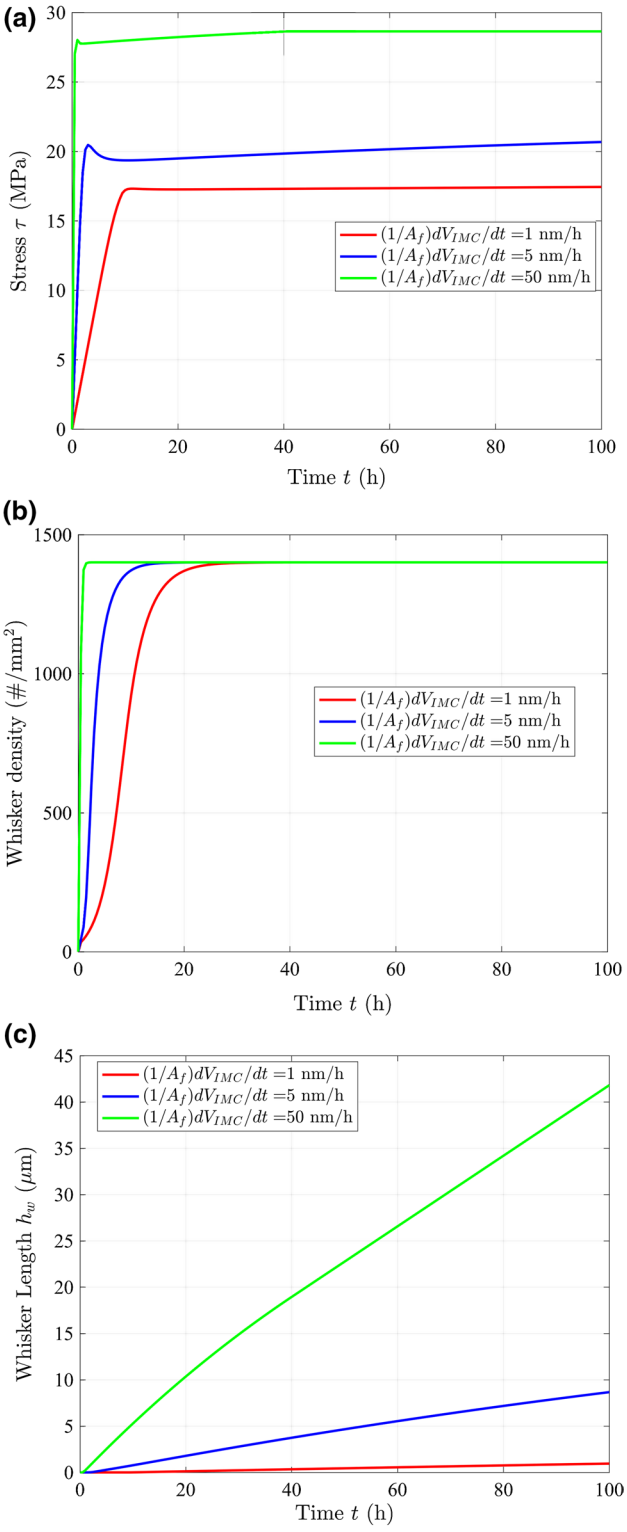

Fig. 13 Predicted (a) stress; (b) whisker density; and (c) whisker length in a Sn film on a Cu substrate, for three different rates of change of intermetallic volume in the film.

they reach the critical length h_0 at which the threshold stress saturates. Finally, if $\tau_{creep} > \tau_{sat}$, whiskers will continue to grow indefinitely. For a film with properties listed in Table I, we find $\tau_{creep} < \tau_0$ for $(1/A_f)dV_{IMC}/dt < 0.56$ nm/h, while $\tau_{creep} < \tau_{sat}$ for $(1/A_f)dV_{IMC}/dt < 4.4$ nm/h. These values are smaller than those typically observed in experiments, but are a similar order of magnitude. Alternatively, we estimate that the threshold stress would need to be increased to 29 MPa to prevent whiskers growing for a typical IMC growth rate of 40 nm/h. These results suggest that relatively small reductions in IMC growth rates, or increases in grain boundary sliding resistance (for example, by solute segregation to the boundaries) may be sufficient to prevent whisker growth. Of course, a model that considers only the average stress and whisker growth rate in the film is likely to underestimate the changes necessary to suppress whiskers altogether, since this would require the growth rates of the fastest whiskers in the statistical distribution to be reduced to zero. Modeling whisker nucleation and growth statistics in more detail may be a fruitful problem for future study.

Conclusions

A recent study[29] reported quantitative measurements of the whisker density and whisker volume in a thin Sn film that was subjected to mechanical pressure over part of its surface. Here, we have described a model of the experiment, with a view to predicting the stress distribution in the film adjacent to the loading area, and correlating the stress with the measured whisker density and length.

The model assumes that stress develops in the film by stress driven grain boundary diffusion from under the punch into the surrounding film. The stress is relaxed by dislocation creep and whisker growth. Whiskers are assumed to form from non-columnar grains, which nucleate by a thermally activated process driven by stress, as described in Ref. 30. They grow by stress-driven diffusion to the base of the whisker. Parameters governing dislocation creep and whisker nucleation were fit to measurements of stress relaxation in a film subjected to thermal loading reported in Ref. 11 leaving three parameters (the pre-exponential for grain boundary diffusion, the attempt frequency for whisker nucleation, and the threshold stress for whisker growth) to be fit to data from the punch experiment.

By comparing the predictions of the model to experiment, we conclude that:

1. For the experimental conditions in Ref. 29, the stress state within 100 μm of the punch reaches a steady-state distribution approximately 10 h after the pressure is applied to the film. The stress has a shallow gradient, decreasing from 25 MPa under the punch to 15 MPa at 100 μm distance from the punch.
2. The model of whisker nucleation proposed in Ref. 11 predicts a whisker density distribution that agrees with experimental measurements for times exceeding 200 h, but underestimates the nucleation rate at early times.
3. The model predicts whisker growth rates adjacent to the punch that are within the scatter of experimental data.
4. Comparison of model predictions with experimental data shows that whiskers grow only if the compressive stress in the film exceeds a critical value. Experiments show that the whisker growth rate decreases with time,[29] which can be explained by an increase in the threshold stress with whisker length. The as-deposited film was estimated to have a threshold stress for whisker growth of 17MPa, increasing to a saturated value of 22 MPa after whiskers reached a length of 19 μm.

Appendix

For completeness, we summarize briefly the numerical procedure that was used to solve the equations governing whisker nucleation and growth listed in the "Model Description" section. The problem must be solved at two separate length-scales. The variation of average stress σ with time and distance from the punch is determined by solving Eq. 2. The solution is coupled to the micro-scale stress field τ (determined by Eqs. 6 and 7) through the average strain rate $\dot{\varepsilon}^I(\sigma)$, which is a function of mean stress σ and also depends on the instantaneous values of whisker area fraction N and the threshold stress for whisker growth τ_{crit}. To solve the coupled equations, the steady-state approximations to Eqs. 6 and 7 were first solved for a range of values of (σ, N, τ_{crit}) and the results were tabulated. This then enabled $\dot{\varepsilon}^I(\sigma)$ to be calculated quickly (by interpolation) while solving Eq. 2. To this end, the governing equations for τ were re-written in dimensionless form, by defining

$$\hat{\tau} = \tau/\Sigma \quad \hat{\sigma} = \sigma/\Sigma \quad \hat{r} = r/L \quad T_0 = \tau_{crit}/\Sigma \tag{19}$$

where L is the grain size and Σ the pressure under the punch. The governing equations for $\hat{\tau}$ then reduce to

$$\begin{cases} +\frac{1}{2}\Gamma(\hat{\tau})^m - \dot{E}^I = 0 & \hat{\sigma} < T_0 \\ -\frac{1}{3}\left(\frac{\partial^2\hat{\tau}}{\partial\hat{r}^2} + \frac{1}{\hat{r}}\frac{\partial\hat{\tau}}{\partial\hat{r}}\right) + \frac{1}{2}\Gamma(|\hat{\tau}|)^m - \dot{E}^I = 0 & \hat{\sigma} > T_0 \end{cases} \tag{20}$$

where Γ is defined in Eq. 16, and

$$\dot{E}^I = \frac{\dot{\varepsilon}^I k T L^2}{\Omega \overline{D} \Sigma} \quad T_0 = \tau_{crit}/\Sigma \tag{21}$$

are dimensionless measures of the strain rate resulting from whisker growth and dislocation creep, and the threshold

stress for whisker growth, respectively. The boundary conditions reduce to

$$\begin{aligned} &\partial\hat{\tau}/\partial\hat{r} = 0 \quad \hat{r} = 1/(2\sqrt{N}) \\ &\hat{\tau} = T_0 \quad \hat{r} = 1/2 \end{aligned} \tag{22}$$

together with the condition for the area average stress

$$\hat{\sigma} = \frac{8N}{(1-N)} \int_{1/2}^{1/(2\sqrt{N})} \hat{\tau}(r)\hat{r}\mathrm{d}\hat{r} \tag{23}$$

To solve the differential equation in (20) it is convenient to recast it, together with (23), as a system of three first-order differential equations, by introducing auxiliary variables

$$\eta(\hat{r}) = \int_{1/2}^{\hat{r}} \hat{\tau}(\xi)\xi\mathrm{d}\xi \quad \theta(\hat{r}) = \frac{\mathrm{d}\hat{\tau}}{\mathrm{d}\hat{r}} \tag{24}$$

With these substitutions, we have

$$\frac{\mathrm{d}\eta}{\mathrm{d}\hat{r}} = \hat{r}\hat{\tau}(\hat{r}) \quad \frac{\mathrm{d}\hat{\tau}}{\mathrm{d}\hat{r}} = \theta(\hat{r}) \quad \frac{\mathrm{d}\theta}{\mathrm{d}\hat{r}} = \frac{\mathrm{d}^2\hat{\tau}}{\mathrm{d}\hat{r}^2} = -\frac{1}{\hat{r}}\theta(\hat{r}) + \frac{3}{2}\Gamma(\hat{\tau})^m - 3\dot{\mathrm{E}}^I \tag{25}$$

with boundary conditions

$$\left.\begin{aligned} \eta &= 0 \\ \hat{\tau} &= T_0 \end{aligned}\right\} \quad \hat{r} = 1/2$$
$$\left.\begin{aligned} \eta &= (1-N)\hat{\sigma}/(8N) \\ \theta &= 0 \end{aligned}\right\} \quad \hat{r} = 1/(2\sqrt{N}) \tag{26}$$

For given values of $\{\hat{\sigma}, N, T_0\}$ Eqs. 25 and 26 may be solved for $\eta, \theta, \hat{\tau}, \dot{\mathrm{E}}^I$. We used the three-stage Lobatto IIIa formula implemented in MATLAB for this purpose.[35] The rates of change of whisker height and volume were then determined from the solution as

$$\frac{\mathrm{d}\hat{h}_w}{\mathrm{d}\hat{t}} = 4\left.\frac{\partial\hat{\tau}}{\partial\hat{r}}\right|_{\hat{r}=1/2} \quad \frac{\mathrm{d}\hat{V}}{\mathrm{d}\hat{t}} = N\frac{\mathrm{d}\hat{h}_w}{\mathrm{d}\hat{t}} \tag{27}$$

where $\hat{h}_\mathrm{w} = (M/\Sigma)h_\mathrm{w}/h_\mathrm{f}$ and $\hat{V}_\mathrm{w} = (M/\Sigma)V_\mathrm{w}/h_\mathrm{f}$ are dimensionless whisker length and whisker volume per unit area, respectively, while

$$\hat{t} = t\left(\frac{M\Omega\overline{D}}{kTL^2}\right) \tag{28}$$

is the dimensionless time scale. In our implementation, $\dot{\mathrm{E}}^I, \hat{h}_\mathrm{w}, \hat{V}_\mathrm{w}$ were computed for 20 equally spaced values of $\hat{\sigma}$ in the range $T_0 < \hat{\sigma} < 1$, and fit by cubic splines. This procedure was repeated for 5 equally spaced values of $\tau_0/\Sigma < T_0 < \tau_\mathrm{sat}/\Sigma$ and 10 values of $N_0 < N < N_\mathrm{sat}$, with spacing determined from $N = N_0\exp(p)$; $0 < p < \log(N_\mathrm{sat}/N_0)$ and p equally spaced.

A simple 1-D finite element method was then used to solve (2) for the variation of mean stress σ adjacent to the punch. For this purpose, it is helpful to re-write (2) in weak form, and in terms of dimensionless variables as,

$$\int_0^{\hat{R}} \frac{\partial\hat{\sigma}}{\partial\hat{t}}\delta\hat{\sigma}\mathrm{d}\hat{x} + \frac{1}{3}\int_0^{\hat{R}} \frac{\partial\hat{\sigma}}{\partial\hat{x}}\frac{\partial\delta\hat{\sigma}}{\partial\hat{x}}\mathrm{d}\hat{x} + \int_0^{\hat{R}} \dot{\mathrm{E}}^I(\hat{\sigma}, N, T_0)\delta\hat{\sigma}\mathrm{d}\hat{x} = 0 \tag{29}$$

Equation 29 was reduced to a system of discrete nonlinear differential equations by interpolating $\hat{\sigma}$ between a set of nodal values $\hat{\boldsymbol{\sigma}}$ using a set of 200 quadratic finite elements over the region $0 < \hat{x} < \hat{R}$. The system was integrated with respect to time using a backward-Euler approximation for $\hat{\boldsymbol{\sigma}}$ and forward-Euler for N and T_0. The discrete system of nonlinear equations for the increment in stress $\Delta\hat{\boldsymbol{\sigma}}$ during a time interval $\Delta\hat{t}$ can be expressed in the form

$$\sum_\mathrm{elements} \int_{\hat{r}_0}^{\hat{r}_1} \mathbf{B}^T\mathbf{q}(\mathbf{B}\left[\hat{\boldsymbol{\sigma}}^n + \Delta\hat{\boldsymbol{\sigma}}\right])\mathrm{d}\hat{x} = 0 \tag{30}$$

where $\hat{\boldsymbol{\sigma}}^n$ is the solution at the end of the preceding time step, while

$$\mathbf{q} = \begin{bmatrix} \frac{\Delta\hat{\sigma}}{\Delta\hat{t}} + \dot{\mathrm{E}}^I(\hat{\sigma}^n + \Delta\hat{\sigma}, N, T_0) \\ \frac{1}{3}\frac{\partial(\hat{\sigma}^n + \Delta\hat{\sigma})}{\partial\hat{x}} \end{bmatrix} \tag{31}$$

and

$$\mathbf{B} = \frac{1}{2}\begin{bmatrix} -(1-\xi)\xi & 2(1-\xi)(1+\xi) & \xi(1+\xi) \\ (2\xi-1)\lambda & -4\xi\lambda & (2\xi+1)\lambda \end{bmatrix} \tag{32}$$

with $\lambda = \mathrm{d}\xi/\mathrm{d}x$ is the finite element interpolation matrix that maps the nodal values of $\boldsymbol{\sigma}$ within an element onto $[\hat{\sigma}, \mathrm{d}\hat{\sigma}/\mathrm{d}\hat{x}]^\mathrm{T}$. Equation 30 can be solved by Newton–Raphson iteration. The linear equations for a correction to $\Delta\hat{\boldsymbol{\sigma}}$ during a generic iteration have the form

$$\left[\sum_\mathrm{elements} \int_{\hat{r}_0}^{\hat{r}_1} \mathbf{B}^T\mathbf{D}\mathbf{B}\mathrm{d}\hat{x}\right]\mathrm{d}\hat{\boldsymbol{\sigma}} = -\sum_\mathrm{elements} \int_{\hat{r}_0}^{\hat{r}_1} \mathbf{B}^T\mathbf{q}(\mathbf{B}\hat{\boldsymbol{\sigma}})\mathrm{d}\hat{x} \tag{33}$$

where the consistent tangent matrix $\mathbf{D}$ is given by

$$\mathbf{D} = \begin{bmatrix} \frac{1}{\Delta\hat{t}} + \frac{\partial\dot{E}^I}{\partial\hat{\sigma}} & 0 \\ 0 & \frac{1}{3} \end{bmatrix} \tag{34}$$

The derivative $\partial\dot{E}^I/\partial\hat{\sigma}$ can be computed by differentiating the spline interpolation for $\dot{\mathrm{E}}^I$

Acknowledgements The authors gratefully acknowledge the support of the NSF-DMR under Contract DMR-1903071.

Conflict of interest The authors declare that they have no conflict of interest.

References

1. G.T. Galyon, and L. Palmer, *IEEE Trans. Electron. Packag. Manuf.* 28, 17 (2005).
2. S.M. Arnold, *Plating* 53, 96 (1966).
3. P. Zhang, Y. Zhang, and Z. Sun, *J. Mater. Sci. Technol.* 31, 675 (2015).
4. R.M. Fisher, L.S. Darken, and K.G. Carroll, *Acta Metall.* 2, 368 (1954).
5. B.Z. Lee, and D.N. Lee, *Acta Mater.* 46, 3701 (1998).
6. W.J. Boettinger, C.E. Johnson, L.A. Bendersky, K.W. Moon, M.E. Williams, and G.R. Stafford, *Acta Mater.* 53, 5033 (2005).
7. E. Chason, N. Jadhav, W.L. Chan, L. Reinbold, and K.S. Kumar, *Appl. Phys. Lett.* 92, 171901 (2008).
8. K.N. Tu, *Phys. Rev. B.* 49, 2030 (1994).
9. K.N. Tu, and R.D. Thompson, *Acta Metall.* 30, 947 (1982).
10. E. Chason, N. Jadhav, and F. Pei, *JOM.* 63, 62 (2011).
11. F. Pei, C.L. Briant, H. Kesari, A.F. Bower, and E. Chason, *Scr. Mater.* 93, 16 (2014).
12. F. Pei, A.F. Bower, and E. Chason, *J. Electron. Mater.* 45, 21 (2016).
13. F. Pei, E. Buchovecky, A. Bower, and E. Chason, *Acta Mater.* 129, 462 (2017).
14. P. Sarobol, J.E. Blendell, and C.A. Handwerker, *Acta Mater.* 61, 1991 (2013).
15. Y. Wang, J.E. Blendell, and C.A. Handwerker, *J. Mater. Sci.* 49, 1099 (2014).
16. M.A. Dudek, and N. Chawla, *Acta Mater.* 57, 4588 (2009).
17. C.H. Pitt, and R.G. Henning, *J. Appl. Phys.* 35, 459 (1964).
18. H. Moriuchi, Y. Tadokoro, M. Sato, T. Furusawa, and N. Suzuki, *J. Electron. Mater.* 36, 220 (2007).
19. S.-K. Lin, Y. Yorikado, J. Jiang, K.-S. Kim, K. Suganuma, S.-W. Chen, M. Tsujimoto, and I. Yanada, *J. Mater. Res.* 22, 1975 (2007).
20. T. Shibutani, Q. Yu, M. Shiratori, and M.G. Pecht, *Microelectron. Reliab.* 48, 1033 (2008).
21. H.P. Howard, J. Cheng, P.T. Vianco, and J.C.M. Li, *Acta Mater.* 59, 1957 (2011).
22. R. Vallabhaneni, E. Izadi, C.R. Mayer, C.S. Kaira, S.S. Singh, J. Rajagopalan, and N. Chawla, *Microelectron. Reliab.* 79, 314 (2017).
23. E. Chason, N. Jadhav, F. Pei, E. Buchovecky, and A. Bower, *Prog. Surf. Sci.* 88, 103 (2013).
24. P. Jagtap, V.A. Sethuraman, and P. Kumar, *J. Electron. Mater.* 47, 5229 (2018).
25. C.-F. Li, and Z.-Q. Liu, *Acta Mater.* 61, 589 (2013).
26. W.J. Choi, T.Y. Lee, K.N. Tu, N. Tamura, R.S. Celestre, A.A. MacDowell, Y.Y. Bong, and L. Nguyen, *Acta Mater.* 51, 6253 (2003).
27. P. Jagtap, A. Chakraborty, P. Eisenlohr, and P. Kumar, *Acta Mater.* 134, 346 (2017).
28. C. Herring, *J. Appl. Phys.* 21, 437 (1950).
29. P. Jagtap, N. Jain, and E. Chason, *Scr. Mater.* 182, 43 (2020).
30. E. Chason, F. Pei, C.L. Briant, H. Kesari, and A.F. Bower, *J. Electron. Mater.* 43, 4435 (2014).
31. P. Singh, and M. Ohring, *J. Appl. Phys.* 56, 899 (1984).
32. K.N. Tu, *Acta Metall.* 21, 347 (1973).
33. E. Buchovecky, N. Jadhav, A.F. Bower, and E. Chason, *J. Electron. Mater.* 38, 2676 (2009).
34. B. Illés, O. Krammer, T. Hurtony, K. Dušek, D. Bušek, and A. Skwarek, *J. Mater. Sci. Mater. Electron.* 31, 16314 (2020).
35. J. Kierzenka, and L.F. Shampine, *ACM Trans. Math. Softw.* 27, 299 (2001).